Military Technical College
Kobry El-Kobbah,
Cairo, Egypt.

16th International Conference on Applied Mechanics and Mechanical Engineering.

MODELING OF DYNAMIC SYSTEMS WITH VIBRO-IMPACT INTERACTION AND DISCONTINUITY MAPPING

R. A. Ibrahim*

ABSTRACT

This paper presents an overview of selected modeling techniques of vibro-impact dynamics. Vibro-impact dynamics has occupied a wide spectrum of studies by dynamicists, physicists, and mathematicians. These studies may be classified into three main categories: modeling, mapping and applications. The main techniques used in modeling of vibro-impact systems include phenomenological modeling, Hertzian models, and non-smooth coordinate transformations developed by Zhuravlev and Ivanov. One of the most critical situations impeded in vibro-impact systems is the grazing bifurcation. Grazing bifurcation is usually studied through discontinuity mapping techniques, which are useful to uncover the rich dynamics in the process of impact interaction. Complex dynamic phenomena of vibro-impact systems such as sub-harmonic oscillations, chaotic motion, and coexistence of different attractors for the same excitation and system parameters but under different initial conditions will be discussed.

KEY WORDS

Non-smooth coordinate transformations, Hertzian contact, power law, mapping, chaotic motion, sub-harmonic oscillation.

* Professor, Wayne State University, Department of Mechanical Engineering, Detroit, MI 48202, USA, ibrahim@eng.wayne.edu

INTRODUCTION

Vibro-impact systems are well known to laymen and children. Simple toys include a skipping stone on the water surface and the woodpecker toy. For skipping to be successful, one has to impart spin to a flat stone with a given angle of attack, which is considered as the most crucial factor. Skipping is associated with slow down due to energy dissipation during collision. The collision process is also associated with angular destabilization. The woodpecker toy operates by self-excited vibrations due to the combined effects of friction, impact and weight. The dynamics of this toy is greatly influenced by simultaneous impacts which cause discontinuous bifurcations. A mass-spring oscillator against one-sided barrier, see **Fig. 1**, and an inverted pendulum oscillating against two-sided barriers are two classical examples of vibro-impact dynamical systems. Practical engineering applications include ship roll motion against one-sided barrier, rotor-stator rubbing/impact, heat exchanger tube fretting due to adjacent tubes interaction, slamming of ocean waves on offshore structures, automotive braking systems, pipes conveying fluid with end-restraints, loosely fitting joints, vocal folds collision, micro-actuators, contact micro-electro-mechanical systems (MEMS) and impact dampers. Generally, vibro-impact systems involve multiple impact interactions in the form of jumps in state space. In most cases, there is energy loss due to impacts and the coefficient of restitution usually measures the degree of energy dissipation associated with an impact event. The time scale involved during impact is much smaller than the time scale of the natural frequency of oscillation. The dynamics of vibro-impact systems are described by strongly nonlinear non-smooth differential equations. These systems usually experience discontinuities in time of the state space due to velocity reversals. The theory of vibro-impact dynamics has been documented in several research monographs (see, e.g., [1, 2]). This paper provides an overview of selected analytical techniques, numerical algorithms, and discontinuity mapping.

POWER-LAW PHENOMENOLOGICAL MODELING

For an assumed rigid impact one must have to introduce the constraint, i.e., $x \leq +x_i$, where x is the system response displacement and x_i is the barrier location (see **Fig. 1**). One can introduce a phenomenological modeling that describes the interaction between the system and barrier with a special potential field of interaction, which is very weak in the region between the body surface and the barrier, $x \leq +x_i$, but becomes fast growing in the neighborhood of the point, $x = +x_i$. The force of interaction can thus phenomeno-logically represented by the power function

$$F_i = b\left(\frac{x}{x_i}\right)^{2n-1} \tag{1}$$

where $n \gg 1$ is an integer and b is a positive constant parameter usually estimated from experimental measurement. Such representation was proposed in vibro-impact problems by Hunt and Crossley [3] and in simulating liquid sloshing impact in moving containers [4-5].

Figure 2 shows the dependence of the impact force on the spatial coordinate, x/x_i, for different values of n for the case of two-sided barrier. For the case of $n \to \infty$, we

have the case of absolutely rigid body interaction, where the corresponding potential energy takes the square well form. For finite and large values of n, the interaction field is not absolutely localized at the points, $x = \pm x_i$. This implies that both the system and barrier are not absolutely rigid, but admit a small deformation at the regions of impact, $x = \pm x_i$, for two-side barriers.

The damping effects during impact are spatially localized around the region, $x = \pm x_i$. The localized dissipative force may also be phenomenologically represented by the expression

$$F_d = d\left(\frac{x}{x_i}\right)^{2p}\dot{x} \tag{2}$$

where d is a constant coefficient to be determined experimentally, $p>>1$ is a positive integer, and a dot denotes differentiation with respect to time.

ZHURAVLEV NONSMOOTH COORDINATE TRANSFORMATIONS

The non-smooth coordinate transformation introduced by Zhuravlev [6] assumes perfectly stiff constraints and converts the vibro-impact system into an oscillator without barriers such that the equations of motion do not contain any impact terms. With reference to **Fig. 3**, the ship roll equation of motion may be written in the form, [7, 8],

$$q'' + \zeta q' + \gamma q'\left|q'\right| + q + C_3 q^3 + C_5 q^5 = Z(\tau) \tag{3}$$

where $q = \phi/\phi_c$, ϕ is the ship roll angle, and ϕ_c is the roll capsize angle. The coefficients $C_3 < 0$, $C_5 > 0$ are usually determined experimentally. ζ and γ are the coefficients of linear and nonlinear damping moments, respectively. The third term of the left hand side is to capture the effects of flow separation and onset of turbulence. Note that the modulus operation, $|q'|$, makes the damping function always odd despite of the presence of its quadratic form. $Z(\tau)$ represents the wave excitation and $\tau = \omega_n t$ is the non-dimensional time parameter, where ω_n is the ship linear roll natural frequency.

Note that the ship model may experience impact when its roll angle reaches the impact angle, $\phi = -\phi_i$ (see **Fig. 3**). For perfectly elastic impact, Zhuravlev transformation may be written in the form

$$q = |z| - q_i \ , \ q_i = \phi_i/\phi_c \tag{4}$$

where z is a new coordinate, which is free from any constraints. This transformation shifts the barrier to the axis $z = 0$ and unfolds the domain $q > -q_i$ of the phase plane trajectories on the original plane (q, q') to the infinite phase plane (z, z'). To account for the damping associated with inelastic impact, one has to introduce the condition $(q'_+ = -eq'_-)$, where e is the coefficient of restitution, and q'_+ and q'_- are the velocities

just after and before impact, respectively. Note that the additional damping associated with inelastic impact may be more significant than the inherent system linear and nonlinear damping terms. In this case, the ship equation of motion may be written in the form

$$z^{''}+\zeta z^{'}+\gamma z^{'}\left|z^{'}\right|+z+\mathrm{sgn}(z)[-q_i+C_3\left(|z|-q_i\right)^3+C_5\left(|z|-q_i\right)^5]+(1-e)z^{'}\left|z^{'}\right|\delta\_(z)=Z(\tau)\,\mathrm{sgn}(z) \qquad (5)$$

where $Z(\tau)=\mathrm{a}\sin\nu\tau$, a is the non-dimensional excitation amplitude, $\nu=\Omega/\omega_n$ is the excitation frequency ratio, $\delta\_$ stands for specific distribution applied to some testing function $\vartheta(t)$ such that $\int_{-\infty}^{\infty}\vartheta(t)\delta\_(t)dt=\vartheta(0\_)$. In contrast to the conventional Dirac delta function, $\delta\_(t)$ takes the value of $\vartheta(t)$ on the left of zero but not exactly at zero. Note that using the classic Dirac delta function in equation (5) would be unjustified due to the discontinuous factor $z^{'}\left|z^{'}\right|$ at $z=0$. Accordingly, the term $(1-e)z^{'}\left|z^{'}\right|\delta\_(z)$ provides only approximate description for the energy loss at the barrier, $z=0$, which is justified under the condition $(1-e)<<1$. Although the model still includes singularity due to the localized energy dissipation, the corresponding term (the last one on the left-hand side of equation (5)) has a relatively small integral effect due to the factor $(1-e)$. This enables one to consider the dissipative term as a perturbation when using averaging tools. Note that, even though impact events have been effectively eliminated by the non-smooth coordinate transformation, direct executions of numerical codes with respect to equation (5) still require conditioning due to the presence of singular dissipation term. In such situation, one may try using the idea of averaging to spread the localized damping over one cycle of motion.

IVANOV NON-SMOOTH COORDINATE TRANSFORMATION

For the case of inelastic impact, Ivanov [9] introduced a non-smooth transformation of state variables including both displacement and velocity. Equation (3) can be written in terms of the state vector form

$$u=q^{'}, \qquad u^{'}=-\zeta q^{'}-\gamma q^{'}\left|q^{'}\right|-q-C_3q^3-C_5q^5+Z(\tau) \qquad (6)$$

Adopting Ivanov non-smooth coordinate transformation in the form

$$q=s\ \mathrm{sgn}(s)-q_i, \qquad u=\mathrm{sgn}(s)[1-K\ \mathrm{sgn}(s\,\upsilon)]\ \upsilon \qquad (7)$$

where s and υ are the new coordinates whose values are not restricted, $K=(1-e)/(1+e)$. Alternatively, equations (7) may be written in the form

$$s=(q+q_i)\ \mathrm{sgn}(s), \qquad \upsilon=\frac{\mathrm{sgn}(s)}{1-K^2}[1+K\ \mathrm{sgn}(s\,\upsilon)]\ u \qquad (8)$$

Taking the time derivative of equations (8), using equations (6) and (7), and consider sinusoidal excitation $Z(\tau)=\mathrm{a}\sin\nu\tau$, gives the ship equation of motion in terms of s and υ coordinates

$$s' = [1 - K\ \mathrm{sgn}(s.\upsilon)]\ \upsilon$$

$$\upsilon' = -\zeta\upsilon - \gamma\upsilon|[1 - K\ \mathrm{sgn}(s\,\upsilon)]\ \upsilon| + \mathrm{sgn}(s)\left[\frac{1 + K\ \mathrm{sgn}(s\,\upsilon)}{1 - K^2}\right]\{-(s\ \mathrm{sgn}(s) - q_i) - C_3(s\ \mathrm{sgn}(s) - q_i)^3 - C_5(s\ \mathrm{sgn}(s) - q_i)^5 + \mathrm{a}\sin\nu\tau\} \quad (9)$$

Equation (9) describes the ship roll dynamics with one-sided inelastic barrier on the entire time interval, where conditions of reflection from the barrier and impact energy loss are already included through transformation (8). The results generated using the two transformations are compared based on the study conducted by Grace et al. [7]. **Figs. 4(a)** and **4(b)** are obtained for the two models and display the ship time history response record, its FFT plot and the system path on the coordinate-velocity plane for the same parameters and initial conditions. A comparison between the plots of **Figs. 4(a)** and **4(b)** reveals that the two transformations yield periodic oscillations in which **Fig. 4(a)** experiences one impact event per one excitation period, while **Fig. 4(b)** exhibits two impacts every three excitation periods. For different initial conditions the two models predict different response regimes. For example, for initial conditions $z_o = 0.39$ and $z'_o = -0.35$, Zhuravlev model yields unstable ship roll motion in the form of ship capsizing, while Ivanov model yields multi-period oscillations with occasional impacts (2 impacts per 3 excitation periods).

The bifurcation diagrams shown in **Figs. 5(a)** and **5(b)** for Zhuravlev (model 1) and Ivanov (model 2), reveal the coexistence of different solutions for the same excitation level depending on initial conditions. The excitation amplitude at which the unbounded motion (ship capsizing) occurs defines the ship stability boundary and depends on the excitation frequency ratio, ν. The stability boundaries for elastic, $e = 1$, and inelastic, $e = 0.8$, impact cases are shown in **Fig. 6**. It is seen that the bounded region of the inelastic impact is expanded than that of the purely elastic impact region due to the inherent damping associated for all cases of $e < 1$. It is more expanded for model 2 than model 1 for the same coefficient of restitution $e = 0.8$.

UNCERTAINTY OF RESTITUTION COEFFICIENT

The dependence of the coefficient of restitution on the relative velocity of impacting bodies was studied in several papers. The velocity dependence of the restitution coefficient was experimentally measured from a collision between two pendulums with a suspension of 2-m [10]. The restitution coefficient was found to decrease with an increase in the colliding velocity as shown in **Fig. 7**. The analytical results are shown by solid curves by using the experimental values at velocity of 0.5 m/s. The analytical results of reference [10] was found in close agreement with experimental results for $e \approx 1$, and the dependence of the coefficient of restitution was given by the relationship

$$e = 1 - Av_i^B \quad (10a)$$

where A and B are positive constants, and v_i is the impact velocity. The agreement was violated for small values of e. Note that this relationship was derived from

models of purely viscoelastic behavior. In reality, there are often other mechanisms of dissipation to consider as well. At high impact velocities, the energy dissipated in the form of elastic waves increases, as does the loss of energy due to plastic deformation [11]. At low impact velocities, the effects of phenomena such as adhesion [12] and gravity become significant [11]. Roux and Dickerson [13] showed that the dependence of the coefficient of restitution on the initial velocity of a tennis ball is governed by a relationship similar to equation (10a) but with uncertainties in its constants. For example, they expressed equation (10a) in the form

$$e = 1 - (0.18 \pm 0.07)(v_i)^{(0.5 \pm 0.1)} \tag{10b}$$

It is seen that the uncertainty in the constants is as much as 40% for the coefficient and 20% for the exponent.

In the kinetic theory of non-adhesive granular matter, it is assumed that the coefficient of restitution is either a constant or monotonically decaying function of the impact velocity (see, e.g., [14-16]). Later, Müller et al. [17] showed that this assumption is not always sufficient to describe the dynamics of collision accurately, since, at least for a certain time part of the kinetic energy of the relative motion can be stored in colliding bodies' vibrations. This conclusion was based on bouncing ball experiments, which revealed unexpected equidistant step-like features in the coefficient of restitution as a function of impact velocity.

The coefficient of restitution was measured from impact tests of small ship wood model against rigid steel barrier [8] using the basic definition $e = \left| \dot{\phi}_+ / \dot{\phi}_- \right|$, where $\dot{\phi}_+$ and $\dot{\phi}_-$ are the ship model velocities just after and before impact, respectively. It was found that the coefficient of restitution e depends also on the velocity just before impact and its value is unrepeatable in every cycle and in every test. Some studies in other applications confirmed this observation. For example, in impact analysis of multibody dynamics considered by Schiehlen and Seifried [18], the multiple impacts in every test were found to be the source of the uncertainty of the coefficient of restitution and depend on the velocity. It was shown that for the case of rod impacts, the coefficient of restitution decreases monotonically with increasing initial velocity. Ronsse and Sepulchre [19] showed that the acceleration of the table with a bouncing ball at impact is an important parameter for the robustness of the feedback system to model uncertainty, in particular to the uncertainty on the coefficient of restitution. **Fig. 8** shows the dependence of the coefficient of restitution on the velocity of the model just before impact. It is seen that the dependence is scatter. The curve fitting of the measured points reveal a monotonic decrease with the impact velocity. The curve fitting was based on selecting the exponential form:

$$e = Exp\left\{ \varsigma_1 \left| \dot{\phi}_- \right| + \varsigma_2 \left| \dot{\phi}_- \right|^2 \right\} \tag{11}$$

where the coefficients ς_1 and ς_2 were chosen to satisfy the boundary conditions $e=1$ at $|\dot{\phi}_-| = 0$ and $e=0$ at $|\dot{\phi}_-| = \infty$.

DISCONTINUITY MAPPINGS

The study of vibro-impact systems has been facilitated by the concept of discontinuity mappings introduced by Nordmark [20]. These mappings approximate the near-grazing impacting dynamics using a discrete dynamical system obtained solely from the conditions at the grazing contact. Chin et al. [21] provided an exhaustive examination of the Nordmark [20] map, and predicted the occurrence of a series of transitions from a non-impacting period-1 orbit to period-M orbits, with $M = 2,3,...$ De Weger et al [22] called this series by *period-adding* transitions. They were able to explore these period-adding transitions experimentally. De Weger, et al. [22] called the *M*-periodic orbits with one impact per period as "*maximal"* periodic orbits. Maximal orbits imply the occurrence of a single impact per period in *M*-periodic orbits.

Mappings that possess a particular form containing a square root term occur as local Poincaré mappings of the type considered by Nordmark [20]. One can develop a mapping for the linear oscillator, see **Fig. 1**,

$$\ddot{x} + 2\zeta\omega_n\dot{x} + \omega_n^2 x = \bar{f}_0 \sin\Omega t \tag{12}$$

Setting $t = (2\pi/\Omega)\tau$, equation (12) may be written in the form

$$x'' + \varsigma x' + \varpi^2 x = f_0 \sin(2\pi\tau) \tag{13}$$

where $f_0 = 4\pi^2\bar{f}_0/\Omega^2$, $\varpi^2 = 4\pi^2\omega_n^2/\Omega^2$, and $\varsigma = 4\pi\zeta(\omega_n/\Omega)$. The mapping from $\tau = n$ to $\tau = n+1$, where n is an integer is a Poincaré map on the plane (x, x') with constant phase and thus has the same set of eigenvalues as the Jacobian matrix of the linear map [20],

$$\begin{cases} x_{n+1} = \alpha x_n + y_n + \Re \\ y_{n+1} = -\gamma x_n \end{cases} \quad for\ x_n \le 0 \tag{14a}$$

$$\begin{cases} x_{n+1} = -\sqrt{x_n} + y_n + \Re \\ y_{n+1} = -\gamma e^2 x_n \end{cases} \quad for\ x_n > 0 \tag{14b}$$

where $\Re$ is a parameter related to the amplitude of the external excitation and e is the coefficient of restitution which measures the energy loss at impact. The parameters α and γ depend on the intrinsic properties of equation (13) such that the limit $\gamma \to 0$ corresponds to large damping coefficient, and $\gamma e^2 = 1$ corresponds to zero dissipation. These parameters were derived by Chin et al. [21] in the form

$$e^{-\varsigma} = \gamma, \qquad 2e^{-\varsigma/2}\cosh\sqrt{\varsigma^2 - 4\varpi^2} = \alpha \tag{15a,b}$$

For positive values of $\varsigma > 0$, we have from equations (15) the bounds $0 < \gamma < 1$, and $0 < \alpha < 1 + \gamma$.

Equation (14a) is the mapping of a system with no impact within one time interval, while equation (14b) belongs to the case of impact occurrence within that period. The term $-\sqrt{x_n}$ signals the effect of impact. Since equations (14a,b) are continuously differentiable except at $x_0 = 0$, the term $-\sqrt{x_n}$ is referred to as square-root singularity because its Jacobian matrix is singular. Chin et al. [21] numerically generated the bifurcation phenomena for the Nordmark map given by equations (14a,b) as the bifurcation parameter $\Re$ increases through $\Re = 0$ (grazing impact). **Figs. 9(a) and 9(b)** show the bifurcation diagrams for $e = 1$, and two sets of the system parameters $(\gamma, \alpha) = (0.05, 0.65)$ and $(0.01, 0.25)$, respectively. Three basic bifurcation scenarios were reported. The first exhibits bifurcation from a stable period-1 orbit for $\Re < 0$ to reversed infinite period adding cascade as $\Re$ increases through zero. For example, **Fig. 9(a)** shows a cascade where chaos appears in bands between successive windows of periodic behavior. On the other hand, **Fig. 9(b)** reveals a cascade with hysteresis. The second case is characterized by bifurcation from a stable period-1 orbit in $\Re < 0$ to chaotic attractor as $\Re$ increases through zero. The third scenario belongs to collision of an unstable period-M maximal orbit (which is a regular saddle, and is created, together with a stable period-M maximal orbit in a saddle-node bifurcation in $\Re < 0$) and the period-1 orbit at $\Re = 0$.

The value of the bifurcation parameter $\Re$ was obtained, using nonlinear and lengthy analysis by Molenaar et al. [23], in the form

$$\Re = \frac{1 - \alpha + \gamma}{2\,|A|\,(1+e)^2 \left[(-e^{s_1} + e^{s_2}) / (s_2 - s_1) \right]^2} \tag{16}$$

where A is the acceleration of the particular solution of the oscillator when the excitation amplitude, F_0, approaches its value, F_g, at grazing impact, i.e., when $\sigma = (F_0 - F_g)/F_g$. $s_{1,2} = \frac{1}{2}\left(-\varsigma \pm \sqrt{\varsigma^2 - 4\varpi^2}\right)$. Molenaar et al. [23] observed that the fixed negative sign that precedes the square root in equation (14b) prohibits period-one maximal periodic orbits for the underdamped oscillator. Their nonlinear analysis yielded the modified form of the transformed map

$$\begin{cases} x_{n+1} = \alpha x_n + y_n + \Re \\ y_{n+1} = -\gamma x_n \end{cases} \quad for\ x_n \le 0 \tag{17a}$$

$$\begin{cases} x_{n+1} = -C_1\sqrt{x_n} + C_2 x_n + y_n + \Re \\ y_{n+1} = C_3 x_n \end{cases} \quad for\ x_n > 0 \tag{17b}$$

where

$$C_1 = sign\left(\frac{-e^{s_1} + e^{s_2}}{s_2 - s_1}\right), \qquad C_2 = \alpha - 2(1+e)\left(\frac{-s_1 e^{s_1} + s_2 e^{s_2}}{s_2 - s_1}\right) + (1+e)^2\left(\frac{-s_1 e^{s_1} + s_2 e^{s_2}}{s_2 - s_1}\right)^2$$
$$C_3 = (1+2e)\gamma - (1+e)^2\left(\frac{-s_1 e^{s_1} + s_2 e^{s_2}}{s_2 - s_1}\right)^3 \tag{18}$$

One may observe a significant difference between the two maps given by equations (14) and (17). For example, the sign factor, C_1, of the square-root guarantees the presence of maximal period-one orbits. The extra term, $C_2 x_n$, in the first equation of (17b), provides a quantitative understanding of the loss of stability of maximal periodic orbits due to an additional impact. The coefficient C_3 is different from that of Nordmark [20].

For the case of flexible barrier the impact mass will penetrate the barrier in a form of elastic deformation. In this case the coefficient of restitution must be within the range, $0 \le e \le 1$. For low-velocity impact, the barrier will have influence when it absorbs energy, which is measured by the value $e < 1$. For this case, Molenaar et al. [23] obtained the same mapping equations (17) but with the following coefficients

$$C_1 = sign\left(\frac{-e^{s_1} + e^{s_2}}{s_2 - s_1}\right), \qquad C_2 = \alpha - 2(1-e)\left(\frac{-s_1 e^{s_1} + s_2 e^{s_2}}{s_2 - s_1}\right) + (1-e)^2\left(\frac{-s_1 e^{s_1} + s_2 e^{s_2}}{s_2 - s_1}\right)^2$$
$$C_3 = (1-2e)\gamma - (1-e)^2\left(\frac{-s_1 e^{s_1} + s_2 e^{s_2}}{s_2 - s_1}\right)^3 \qquad (19)$$

For a non-impact regime the map is linear. However, the impact orbit possesses a square-root singularity. Close to grazing, the acceleration near impact can be considered constant and the square-root is simply the relationship between elapsed time and traveled distance in systems with constant acceleration. The square-root singularity and the associated extreme stretching of phase space near the point of grazing impact lead to highly non-trivial dynamics.

CONCLUSIONS

Three different and powerful modeling techniques of vibro-impact dynamics have been represented in this article. Other techniques less frequently employed in the literature include Hertzian contact, non-smooth time transformation and time-wise mapping. These methods are well documented and demonstrated by Ibrahim [2]. Experimental measurements of vibro-impact systems under sinusoidal excitation revealed that the coefficient of restitution is uncertain parameter and is monotonically decreasing with the impact speed. In modeling vibro-impact systems, the coefficient of restitution must be represented by a random variable dependent on the impact velocity. The analysis of vibro-impact systems in this case must be performed numerically using Monte-Carlo simulation.

REFERENCES

[1] Babitsky, V. I., Theory of Vibro-Impact Systems: Approximate Methods, Springer-Verlag, Berlin, (1998).

[2] Ibrahim, R. A., Vibro-Impact Dynamics: Modeling, Mapping and Applications, Springer-Verlag, Berlin, (2009).

[3] Hunt, K. H. and Crossley, F. R. E., "Coefficient of restitution interpreted as damping in vibro-impact," ASME J. of Appl. Mech, Vol. 97, pp 440-445, (1975).
[4] Pilipchuk, V. N. and Ibrahim, R. A., "The dynamics of a nonlinear system simulating liquid sloshing impact in moving structures," J. of Sound and Vibr., Vol. **205**, pp 593-615, (1997).
[5] Ibrahim, R. A. and El-Sayad, M. A., "Simultaneous parametric and internal resonances in systems involving strong nonlinearities," J. of Sound and Vibr., Vol. 225, pp 857-885, (1999).
[6] Zhuravlev, V. F., 1976, "Investigation of certain vibro-impact systems by the method of non-smooth transformations," Soviet Mech. of Solids, Vol. **12**, pp. 24-28, (1976).
[7] Grace, I. M., Ibrahim, R. A., and Pilipchuk, V. N., "Inelastic Impact Dynamics of Ships with One-Sided Barriers, Part I: Analytical and Numerical Investigations," Nonlin. Dyn., Vol. **66**(4), pp. 589-607, (2011).
[8] Grace, I. M., Ibrahim, R. A., and Pilipchuk, V. N., "Inelastic Impact Dynamics of Ships with One-Sided Barriers, Part II: Experimental Validation," Nonlin. Dyn., Vol. **66**(4), pp. 608-623, (2011).
[9] Ivanov, A. P., "Impact oscillations: Linear theory of stability and bifurcations," J. of Sound and Vibr., Vol. **178**(3), pp. 361-378, (1994).
[10] Kuwabara, G. and Kono K., "Restitution coefficient in a collision between two spheres," Japanese J. of Appl. Phys., Vol. **26**(8), pp. 1230-1233, (1097).
[11] Falcon, E.; Laroche C.; Fauve S. and Coste C., "Behavior of one elastic ball bouncing repeatedly off the ground," The Europ. Phys. J. B, Vol. **3**, pp. 45-57, (1998).
[12] Ramírez, Rosa; Pöschel Thorsten; Brilliantov Nikolai V. and Schwager Thomas, "Coefficient of restitution of colliding viscoelastic spheres," Phys. Rev. E, Vol. **60**(4), pp. 4465-4472, (1999).
[13] Roux, A. and Dickerson, J., "Coefficient of restitution of a tennis ball," Inter. School of Bangkok (ISB) J. of Physics, Vol. **1**(1), pp. 1-7, (2007).
[14] Lun, C. K., and Savage, S. B., "The effects of an impact velocity dependent coefficient of restitution on stresses developed by sheared granular materials," Acta Mechanica, Vol. **63**, pp. 15-44, (1986).
[15] Luding, S., Clément, E., Rajchenbach, J., and Duran, J., "Simulations of pattern formation in vibrated granular media," Europhyis. Lett., Vol. **36**(4), pp. 247-252, (1996).
[16] Brilliantov, N. V., Salueña, C., Schwager, T., and Pöschel, T., "Transient stresses in a granular gas," Phys. Rev. Lett., Vol. **93**, 134301, (4p.), (2004).
[17] Müller, P., Heckel, M., Sack, A., and Pöschel, T., "Complex velocity dependence of the coefficient of restitution of a bouncing ball," Phys. Rev. Lett., Vol. **110**, 254301 (5p.), (2013).
[18] Schiehlen, W., Seifried, R., "Impact systems with uncertainty," In: Proceedings IUTAM Symposium on Dynamics and Control of Nonlinear Systems, Springer, Berlin, pp. 33-44, (2007).
[19] Ronsse, R., Sepulchre, R., "Feedback control of impact dynamics: The bouncing ball revisited," Proceedings 45th IEEE Conference on Decision and Control, San Diego, CA, pp. 4807-4812, (2006).
[20] Nordmark, A. B., "Non-periodic motion caused by grazing incidence in an impact oscillator," J. of Sound and Vibr. **145**, pp. 279-297, (1991).

[21] Chin, W., Ott, E., Nusse, H. E., and Grebogi, C., "Grazing bifurcations in impact oscillators," Phys. Rev. E, Vol. **50**, pp. 4427-4444, (1994).
[22] De Weger, J., Water, van de W., and Molenaar, J., "Grazing impact oscillations," Phys. Rev. E, Vol. **62**(2), pp. 2030-2041, (2000).
[23] Molenaar, J., de Weger, J. G., and van de Water, W., "Mapping of grazing-impact oscillators," Nonlinearity, Vol. **14**, pp. 301-321, (2001).

Figures:

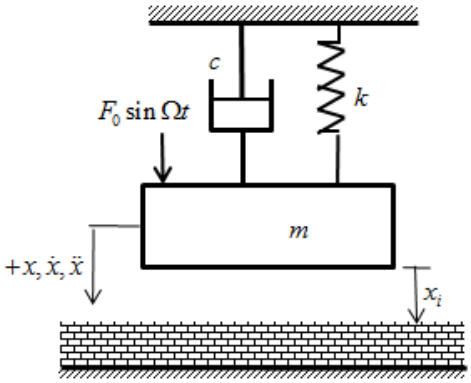

Fig. 1. Schematic diagrams of mass-spring systems with one-sided barrier

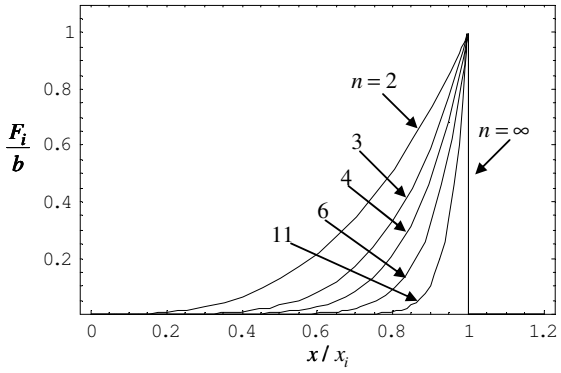

Fig. 2. Spatial dependence of impact for different exponent values for one sided barrier.

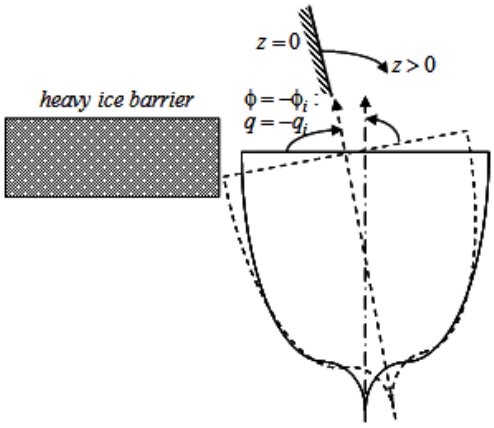

Fig.3. Ship rolls against one-sided barrier.

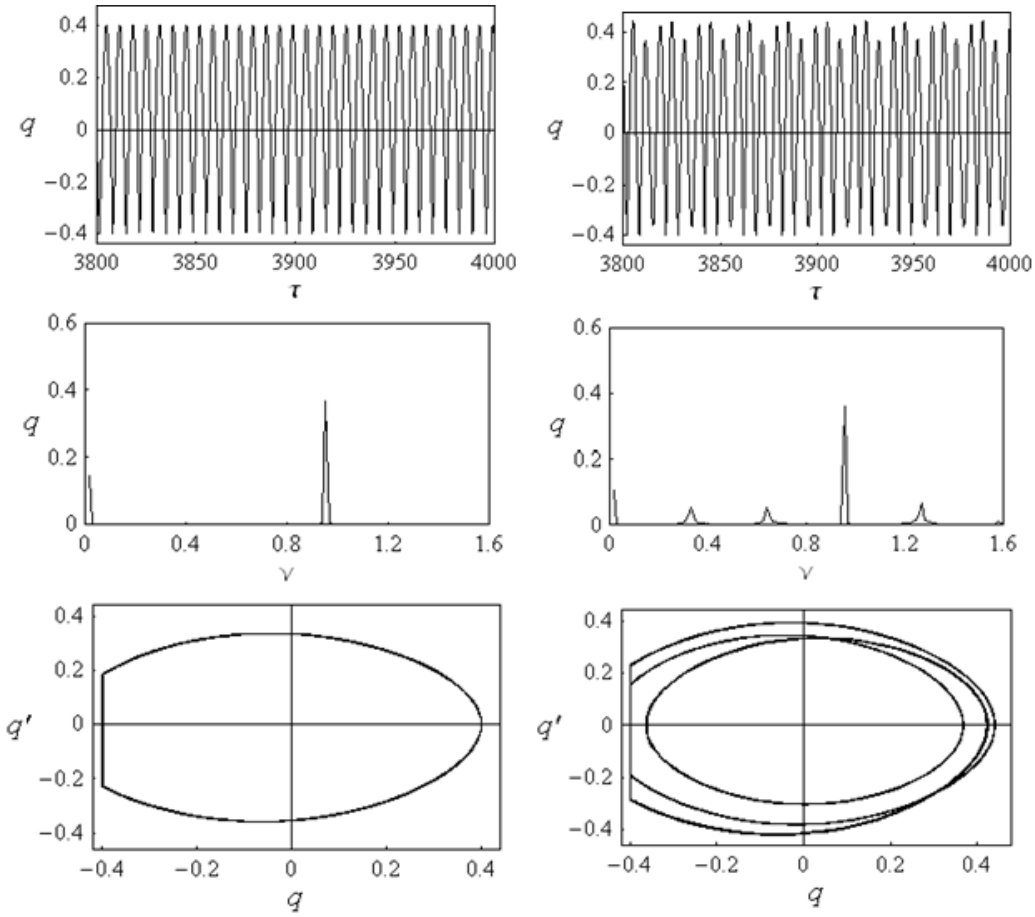

Fig. 4. Ship time history records, FFT plots, and phase portraits, according to (a) Zhuravlev, and (b) Ivanov, for $\nu = 0.94$, $a = 0.08$, $e = 0.8$, and initial conditions $z_0 = 0.01,\ z'_0 = 0.01$. [7]

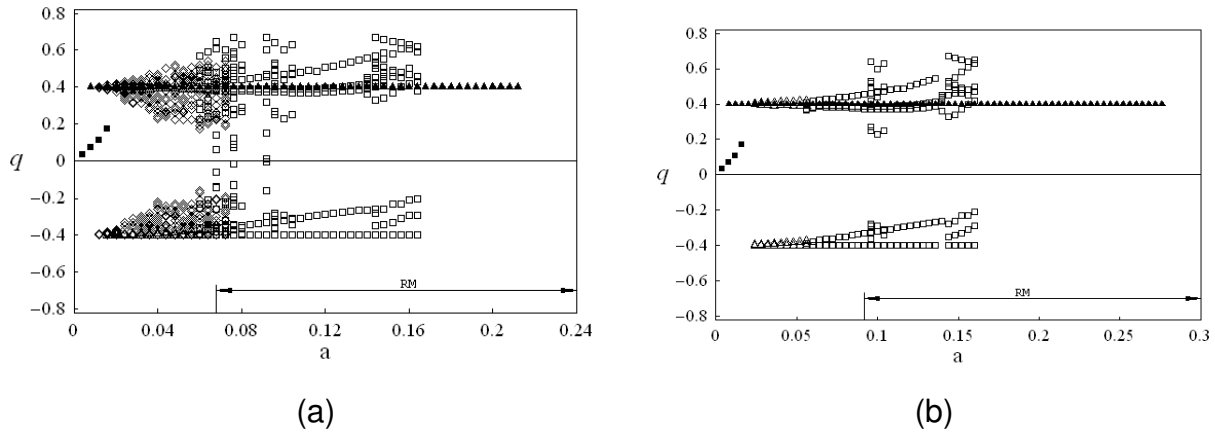

Fig. 5. Bifurcation diagrams for $\nu = 0.94$, and $e = 0.8$; according to (a) Zhuravlev model, and (b) Ivanov model. ■ Period-one response, ▲Period - one response experiencing impact, ∆ Period doubling, ◊ Modulated response, □ Multi - periodic response, and RM= Rotational Motion. [7]

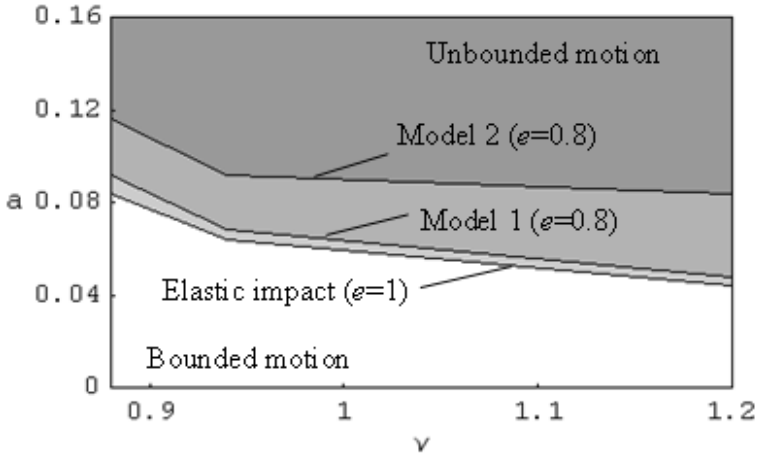

Fig. 6. Estimates for stability boundaries due ship elastic impact, $(e=1)$, and inelastic impact $(e=0.8)$ as predicted by Zhuravlev Model 1 and Ivanov Model 2. Unbounded motion is shown by grey area. [7]

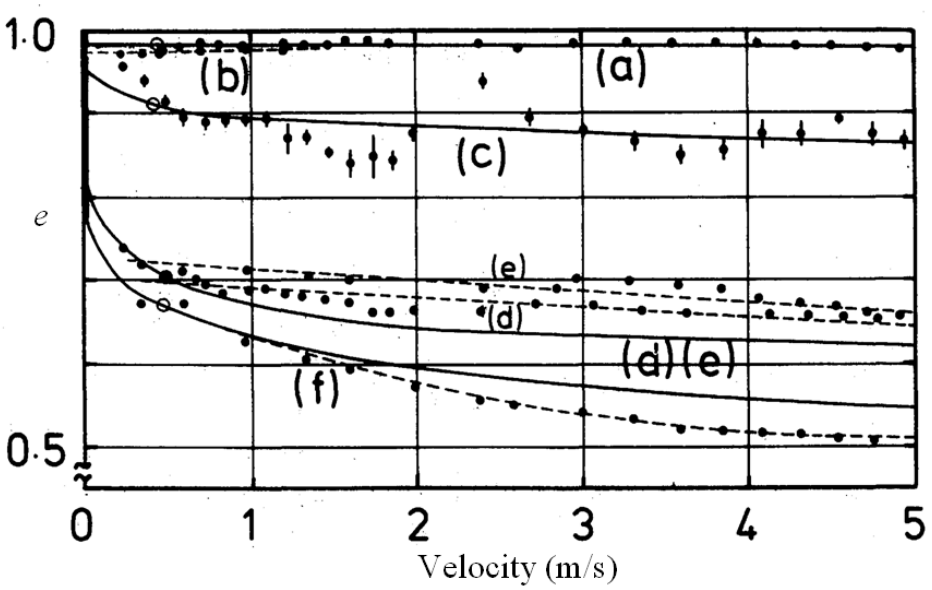

Fig. 7. Dependence of the coefficient of restitution on the velocity. - - - measured values, —— estimated results: (a) Collision between steel sphere of mass $m=0.154$ kg, radius $R=0.0165$ m ; (b) glass spheres $m=0.0333$ kg, $R=0.0196$ m (fractured at high velocity); (c) brass spheres $m=0.119$ kg, radius $R=0.015$ m (plastic deformation at high speed); (d) cork spheres $m=0.0317$ kg, (with a lead core), $R=0.0166$ m ; (e) glass and cork spheres; (f) steel sphere and cork plate (*0.01 m* thick and backed by a heavy iron block. [10]

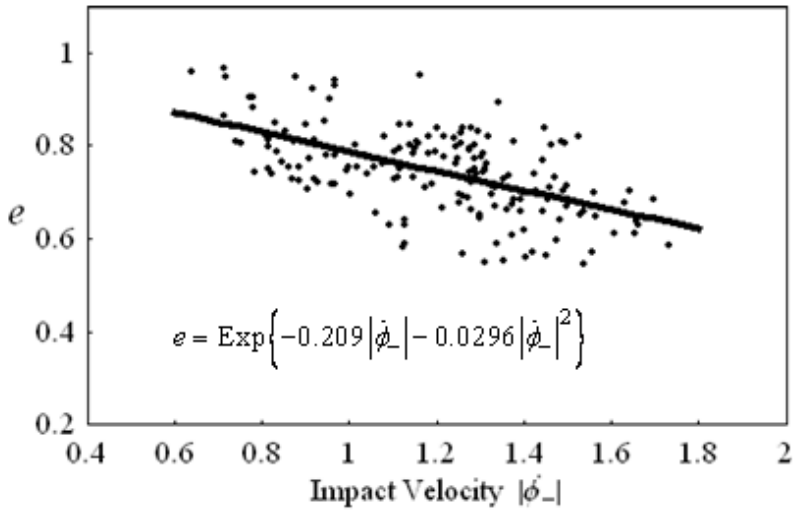

Fig. 8. Dependence of the coefficient of restitution on the impact velocity (the fitting curve is exponential: $e = \mathrm{Exp}\left\{-0.209\left|\dot{\phi}_-\right| - 0.0296\left|\dot{\phi}_-\right|^2\right\}$ [8]

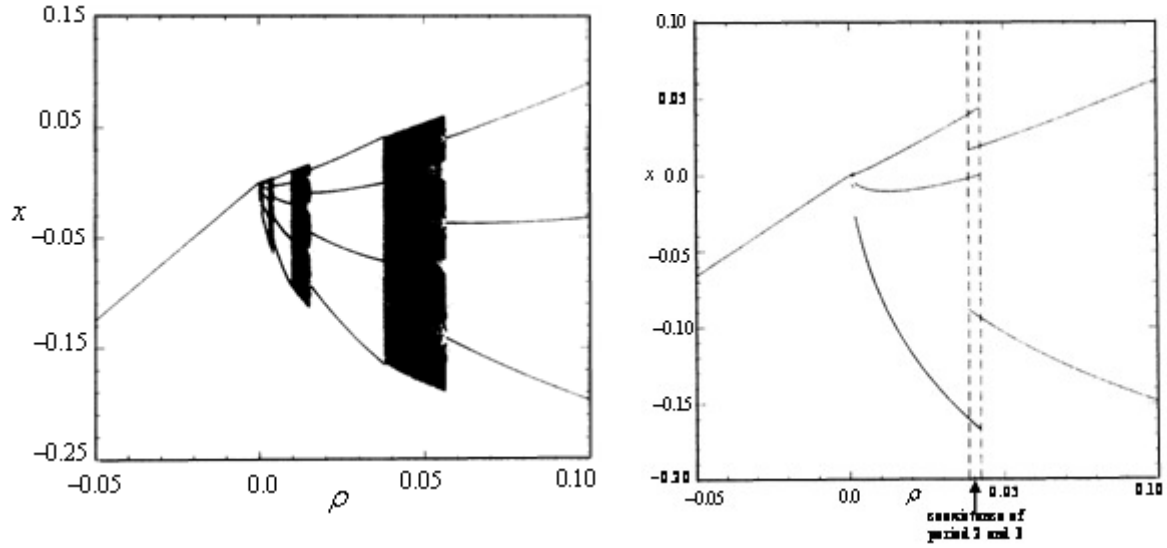

Fig. 9. Bifurcation diagrams for $e = 1.0$: (a) $(\gamma, \alpha) = (0.05, 0.65)$ and (b) $(\gamma, \alpha) = (0.01, 0.25)$, [21].